Measuring SPIO and Gd contrast agent magnetization using 3T MRI

Citation: Cantillon-Murphy, Padraig, Lawrence L. Wald, and Markus Zahn. "Measuring SPIO and Gd contrast agent magnetization using 3T MRI." NMR in Biomedicine 22.8 (2009): 891-897.

As Published: http://dx.doi.org/10.1002/nbm.1412

Publisher: John Wiley & Sons, Ltd.

Persistent URL: http://hdl.handle.net/1721.1/49490

Version: Author's final manuscript: final author's manuscript post peer review, without publisher's formatting or copy editing

Measuring SPIO and Gd contrast agent magnetization using 3T MRI

Short title: Measuring SPIO and Gd contrast agent magnetization using 3T MRI

Pádraig Cantillon-Murphy[1,2], Lawrence L. Wald[3], Markus Zahn[2], Elfar Adalsteinsson[2,3,4]

[1]Division of Gastroenterology, Brigham and Womens' Hospital, Boston, MA.

[2]Department of Electrical Engineering and Computer Science,
Massachusetts Institute of Technology, Cambridge, MA

[3] MGH/HST Athinoula A. Martinos Center for Biomedical Imaging, Charlestown, MA.

[4]Harvard-MIT Division of Health Science and Technology, Cambridge, MA

Correspondence to:

Pádraig Cantillon-Murphy

Brigham and Womens' Hospital,

75 Francis Street, Thorn Room 1123,

Boston, MA 02115, USA.

Phone: 617-732-5925

Email: padraig@mit.edu

Abstract

Traditional methods of measuring magnetization in magnetic fluid samples, such as vibrating sample magnetometry (VSM), are typically limited to maximum field strengths of about 1 T. This work demonstrates the ability of MRI to measure the magnetization associated with two commercial MRI contrast agents at 3 T by comparing analytical solutions to experimental imaging results for the field pattern associated with agents in cylindrical vials. The results of the VSM and fitted MRI data match closely. The method represents an improvement over VSM measurements since results are attainable at imaging field strengths. The agents investigated are Feridex, a superparamagnetic iron oxide suspension used primarily for liver imaging, and Magnevist, a paramagnetic, gadolinium-based compound used for tumors, inflammation and vascular lesions. MR imaging of the agents took place in sealed cylindrical vials in the presence of a surrounding volume of deionized water where the effects of the contrast agents had a measurable effect on the water's magnetization in the vicinity of the compartment of contrast agent. A pair of phase images were used to reconstruct a B_0 fieldmap. The resultant B_0 maps in the water region, corrected for shimming and container edge effects, were used to predict the agent's magnetization at 3 T. The results were compared with the results from VSM measurements up to 1.2 T and close correlation was observed. The technique should be of interest to those seeking quantification of the magnetization associated with magnetic suspensions beyond the traditional scope of VSM. The magnetization needs to be sufficiently strong ($M_s \gtrsim 50$ Am^2/kg Fe for Feridex and $\chi_m \gtrsim 5 \times 10^{-5}$m^3/kg Gd for Magnevist) for a measurable dipole field in the surrounding water. For this reason, the technique is mostly suitable for undiluted agents.

Keywords: Magnetization, MRI, contrast agents, vibrating sample magnetometry, Feridex, Magnevist, dipole field.

1 Introduction

The goal of this work was to demonstrate the ability of MRI to accurately measure the magnetization associated with two commercial MRI contrast agents. These agents were Feridex (AMAG Pharmaceuticals, Cambridge, MA), a superparamagnetic iron oxide suspension used primarily for liver imaging and increasingly for cell-labeling applications [1, 2, 3, 4, 5] and Magnevist (Bayer HealthCare AG, Leverkausen, Germany) [6, 7, 8], a paramagnetic, gadolinium-based (Gd) compound used in a wide variety of tumor and lesion imaging applications.

The investigations used two distinct methods to measure magnetization: vibrating sample magnetometry (VSM) and MRI. VSM measures the sample's magnetization by moving the sample back and forth at high speed, creating a periodically and rapidly changing magnetic field. This changing field is sensed by a set of pick-up coils where the induced coil voltage, as given by Faraday's law of electromagnetic induction, is proportional to the sample's magnetization. While high field VSM platforms exist (*e.g.,* the EV11 system from ADE Magnetics has a 3.1 T maximum field), cost considerations will generally limit VSM use among the MRI community to small samples at fields $\leq$1 T, well below fields currently typical in MRI (*e.g.,* 3 T).

This method comes in the wake of measurements of magnetic susceptibility of gadolinium contrast agents and blood susceptibility conducted by Weisskoff [11]. Jung [12] also made preliminary measurements of the magnetization associated with both Gd-DPTA (now commercially available as Magnevist) and Ferumoxide suspensions (now commercially available as Feridex). Neither investigation examined magnetization at 3 T or used commercially available agents. Chu et al. [13] has described the theoretical "bulk magnetic susceptibility shift" due to an infinite cylinder of finite wall thickness in two field orientations (parallel and perpendicular to B_0). In fact, the "susceptibility shift" refers to the change in the local magnetic field in the region immediately surrounding a paramagnetic species. Bowen et al. [14] have provided a thorough investigation of superparamagnetic iron-oxide loaded cells at 1.89 T by comparing experimental results with the theoretical predictions

of Chu [13] for infinitely long cylindrical vessels of magnetic fluid. More recently, focus has switched to the applications in susceptibility weighted imaging *in vivo* although the technique is broadly similar to that employed here [15, 16].

This work proposes an effective method for predicting the magnetization of Feridex and Magnevist contrast agents using MRI. The experiments are conducted at 3 T but the method could be equally applied at any field strength. The experimental results (both MRI and VSM) are compared with exact theoretical predictions for infinite length cylinders to correlate the magnetization associated with the samples of Feridex and Magnevist. Close correspondence is observed between the MRI results, results from VSM measurements at 1.2 T and previously published results [11]. This technique represents an advancement over prior work in three important respects; (i) it represents the first investigations of commercially available MRI agents, Feridex and Magnevist, (ii) the investigations are the first conducted at 3 T and (iii) the exact rather than an approximate solution [13, 14] for infinite length cylinders is employed.

2 Experimental

2.1 VSM Measurements

To examine magnetic saturation effects in a commercial SPIO contrast agent, 0.0703 cc of Feridex MRI contrast agent was placed in a vibrating sample magnetometer (Model 1660, ADE Magnetics, Westwood, MA) and the magnetic moment was measured. The contrast agents were examined in their undiluted states (*i.e.,* as provided by the manufacturers [2, 6]). To account for magnetization effects due to the sample cup, a second VSM measurement was conducted in the absence of the contrast agent with an empty cup and the resulting magnetization was subtracted from the result in the presence of the agent. The contrast agents' magnetizations are shown in Figure 1(a) where the units of magnetic moment are given as $\mathrm{Am}^2/\mathrm{kg}$ of Fe. Feridex is a superparamagnetic agent which saturates at high field. The saturation magnetization of the agent was estimated to be in the region

of 82 Am^2/kg Fe. Feridex has a nominal density of 11.2 mg Fe/ml and and the recommended dosage is 0.56 mg Fe/kg of bodyweight [2]. A similar procedure was employed for a 0.07266 cc sample of Magnevist contrast agent. Magnevist is a paramagnetic agent which exhibits a linear magnetic susceptibility up to DC fields of 50 T [9]. It consists of a complex chemical formulation, supplied in concentrations containing 469.01 mg gadopentetate dimeglumine per ml Magnevist [6]. The recommended dosage is 0.2 ml per kg bodyweight. The mass susceptibility, χ_m, was estimated by a linear curve fit to be 2.06×10^{-6} m^3/kg Gd from the VSM measurements shown in Figure 1(b). Again, there was no available data beyond 1.2 T. The two VSM measurements took on the order of 1 hour (determined by the iteration step in field strength) to complete without additional postprocessing of the results to determine the magnetic moment per unit volume. Repeated experiments might improve accuracy by adding error bars but this was not attempted.

2.2 MRI Measurements

In order to estimate the magnetization in MRI, B_0 maps were obtained in a 3 T Siemens Trio MRI. The agent was placed in a long, narrow NMR tube (Bruker Match System NMR Sample Tubes from Norell Inc., Landisville, NJ): 10 cm in length and 3.43 mm inner diameter. The walls of the tube were 0.41 mm thick. The tube was fixed to lie horizontally in a water tank for imaging and positioned so that the B_0 field lay transverse to the tube's long axis. The tube's center slice was imaged in coronal view at 3 T with an imaging resolution of 256×256 pixels, a 180mm FOV, a slice thickness of 7 mm and a repetition time, TR = 100 ms. Using 10 averages, the total scan time was 4.25 minutes. The phase maps and B_0 maps are shown in Figures 2 and 3 for the Feridex contrast agent, where TE = 2.83 ms for the phase map and ΔTE = 0.9 ms for the B_0 map. The B_0 map was corrected for edge effects and shimming by taking a second B_0 map in the absence of the tube and identical imaging parameters including the same shimming fields. The second B_0 map was then subtracted from that due to the tube. The original result before correction is shown in Figure 2 for the Feridex agent. The corrected B_0 map is shown in Figure 3. For the MRI measurements, both

contrast agents were examined in their undiluted concentrations to ensure maximum SNR in the resulting images. An identical procedure was employed to obtain a similar result for the Magnevist agent. Simplistic phase unwrapping (Matlab "unwrap" command) was employed but was found to be insufficient due to the complex spatial dependence of the phase in Figures 2 and 3. By utilizing the tolerance parameter of the Matlab "unwrap" command, the regions where no phase wrapping occurred were identified.

2.3 Theoretical Solutions for Infinitely Long Cylinders

The theoretical solution for the magnetic fields associated with an NMR vial placed transverse to the B_0 field is analytically tractable assuming that the cylinder is infinite in length. This is a more than adequate assumption for the finite-length cylinders used in subsequent experiments where the length:inner diameter ratio was 29. For the case of the paramagnetic gadolinium agents, the problem is a two-dimensional, three-region problem where the magnetic susceptibilities of the three regions are χ_1, χ_2 and χ_3. In this work, χ_1 corresponds to the region of contrast agent ($0 < r < R_1$), χ_2 is the glass vial ($R_1 < r < R_2$) and χ_3 is the water region ($r > R_3$), r is the radial displacement from the center of the vial and R_1 and R_2 are the inner and outer radii of the long glass tube. For the case of the SPIO Feridex agent, the region of the contrast agent ($0 < r < R_1$) is considered to have a spatially-invariant magnetization which is colinear with B_0 and has magnitude M_s. This case is explored later.

For an infinitely long vial, simplification arises with the consideration of a two-dimensional cylindrical coordinate set (r, ϕ) and the definition of a transverse magnetic scalar potential, $\Psi(r, \phi)$, for a non-conducting medium such that $\nabla \times \boldsymbol{H} = \mathbf{0}$ and $\boldsymbol{H} = -\nabla\Psi$. In addition, $\nabla \cdot \boldsymbol{B} = \mu_0 \nabla \cdot (\boldsymbol{H} + \boldsymbol{M}) = 0$. For region 1 ($0 < r < R_1$) in this work, $\nabla \cdot \boldsymbol{H} = 0$ whether (i) $\boldsymbol{M} = \chi \boldsymbol{H}$ where $\chi = \chi_1$ is taken to be the spatially uniform magnetic susceptibility of the gadolinium contrast agent, or (ii) $|\boldsymbol{M}| = M_s$ where M_s is the resulting magnetization of the contrast agent which is a function of and parallel to $\boldsymbol{H}$ as given by the Langevin relation for the SPIO contrast agent at 3 T. In practice, SPIO contrast

agents are magnetically saturated at high fields so M_s is virtually independent of $\boldsymbol{H}$ at 3 T. The relation $\nabla \cdot \boldsymbol{H} = 0$ is also true in regions 2 and 3 since these are linearly magnetizable regions with magnetic susceptibilities of χ_2 and χ_3 respectively. Under these conditions, Ψ obeys Laplace's equation, given in (1). Ψ is independent of z for infinitely long cylinders.

$$\nabla^2 \Psi = 0 \tag{1}$$

Eq. (1) has solutions in a cylindrically symmetric geometry as given by Eq. (2) where C_1, D_1, C_2, D_2, C_3 and D_3 are constants to be evaluated by means of boundary conditions at $r = R_1$ and R_2.

$$\Psi(r,\varphi) = \begin{cases} (C_1 r + \frac{D_1}{r}) \cos\varphi & \text{for} \quad 0 < r < R_1 \\ (C_2 r + \frac{D_2}{r}) \cos\varphi & \text{for} \quad R_1 < r < R_2 \\ (C_3 r + \frac{D_3}{r}) \cos\varphi & \text{for} \quad r > R_2 \end{cases} \tag{2}$$

Since Ψ cannot yield infinite field solutions at $r = 0$, we conclude that D_1 =0. The components of $\boldsymbol{H}$ might be written using the gradient operator in cylindrical coordinates, as in Eq. (3), where $\boldsymbol{i}_r$ and $\boldsymbol{i}_\varphi$ are unit vectors in the two-dimensional cylindrical coordinate system.

$$\boldsymbol{H}(r,\varphi) = -\nabla\Psi = \begin{cases} -(C_1 - \frac{D_1}{r^2}) \cos\varphi \boldsymbol{i}_r + (C_1 + \frac{D_1}{r^2}) \sin\varphi \boldsymbol{i}_\varphi & \text{for} \quad 0 < r < R_1 \\ -(C_2 - \frac{D_2}{r^2}) \cos\varphi \boldsymbol{i}_r + (C_2 + \frac{D_2}{r^2}) \sin\varphi \boldsymbol{i}_\varphi & \text{for} \quad R_1 < r < R_2 \\ -(C_3 - \frac{D_3}{r^2}) \cos\varphi \boldsymbol{i}_r + (C_3 + \frac{D_3}{r^2}) \sin\varphi \boldsymbol{i}_\varphi & \text{for} \quad r > R_2 \end{cases} \tag{3}$$

The corresponding components of the **B** field solutions are given by Eq. (4) for a linearly magnetizable region 1.

$$\boldsymbol{B}(r,\varphi) = \begin{cases} -\mu_0(1+\chi_1)(C_1 - \frac{D_1}{r^2}) \cos\varphi \boldsymbol{i}_r + \mu_0(1+\chi_1)(C_1 + \frac{D_1}{r^2}) \sin\varphi \boldsymbol{i}_\varphi & \text{for} \quad 0 < r < R_1 \\ -\mu_0(1+\chi_2)(C_2 - \frac{D_2}{r^2}) \cos\varphi \boldsymbol{i}_r + \mu_0(1+\chi_2)(C_2 + \frac{D_2}{r^2}) \sin\varphi \boldsymbol{i}_\varphi & \text{for} \quad R_1 < r < R_2 \\ -\mu_0(1+\chi_3)(C_3 - \frac{D_3}{r^2}) \cos\varphi \boldsymbol{i}_r + \mu_0(1+\chi_3)(C_3 + \frac{D_3}{r^2}) \sin\varphi \boldsymbol{i}_\varphi & \text{for} \quad r > R_2 \end{cases} \tag{4}$$

The constants are solved by considering the boundary conditions as follows:

$$\begin{aligned}
&\boldsymbol{H}(r \to 0) = finite, \Rightarrow D_1 = 0 \\
&B_r(r = R_1^-) = B_r(r = R_1^+) \\
&B_r(r = R_2^-) = B_r(r = R_2^+) \\
&H_\varphi(r = R_1^-) = H_\varphi(r = R_1^+) \\
&H_\varphi(r = R_2^-) = H_\varphi(r = R_2^+) \\
&\boldsymbol{H}(r \to \infty) = H_0 \boldsymbol{i}_x = H_0(\cos\varphi \boldsymbol{i}_r - \sin\varphi \boldsymbol{i}_\varphi) \; where \; H_0 = \tfrac{B_0}{\mu_0(1+\chi_3)}
\end{aligned} \tag{5}$$

Applying these boundary conditions to Eqs. (3) and (4) yields the following solutions for C_1 through D_3 as given in Table 1(a).

Table 1: Table of Coefficients

Coefficient	(a) Gadolinium agent ($\boldsymbol{M} = \chi_1 \boldsymbol{H}$)	(b) SPIO agent ($\boldsymbol{M} = M_s \frac{\boldsymbol{H}}{\lvert\boldsymbol{H}\rvert}$)
C_1	$\frac{-4H_0\, R_2^2(1+\chi_2)(1+\chi_3)}{R_1^2(\chi_1-\chi_2)(\chi_2-\chi_3)+R_2^2(2+\chi_1+\chi_2)(2+\chi_2+\chi_3)}$	$\frac{4H_0 R_2^2(1+\chi_2)(1+\chi_3)-M_s(R_1^2(\chi_2-\chi_3)+R_2^2(2+\chi_2+\chi_3))}{R_1^2\chi_2(\chi_2-\chi_3)-R_2^2(2+\chi_2)(2+\chi_2+\chi_3)}$
D_1	0	0
C_2	$\frac{-2H_0\, R_2^2(2+\chi_1+\chi_2)(1+\chi_3)}{R_1^2(\chi_1-\chi_2)(\chi_2-\chi_3)+R_2^2(2+\chi_1+\chi_2)(2+\chi_2+\chi_3)}$	$-\frac{M_s R_1^2(\chi_2-\chi_3)-2H_0R_2^2(2+\chi_2)(1+\chi_3)}{R_1^2\chi_2(\chi_2-\chi_3)-R_2^2(2+\chi_2)(2+\chi_2+\chi_3)}$
D_2	$\frac{2H_0\, R_1^2R_2^2(\chi_1-\chi_2)(1+\chi_3)}{R_1^2(\chi_1-\chi_2)(\chi_2-\chi_3)+R_2^2(2+\chi_1+\chi_2)(2+\chi_2+\chi_3)}$	$-\frac{R_1^2R_2^2(-2H_0\chi_2(1+\chi_3)+M_s(2+\chi_2+\chi_3))}{R_1^2\chi_2(\chi_2-\chi_3)-R_2^2(2+\chi_2)(2+\chi_2+\chi_3)}$
C_3	$-H_0$	$-H_0$
D_3	$\frac{H_0\, R_2^2(R_2^2(2+\chi_1+\chi_2)(\chi_2-\chi_3)+R_1^2((\chi_1-\chi_2)(2+\chi_2+\chi_3)))}{R_1^2(\chi_1-\chi_2)(\chi_2-\chi_3)+R_2^2(2+\chi_1+\chi_2)(2+\chi_2+\chi_3)}$	$-\frac{R_2^2(2M_sR_1^2(1+\chi_2)-H_0(-R_2^2(2+\chi_2)(\chi_2-\chi_3)+R_1^2\chi_2(2+\chi_2+\chi_3)))}{R_1^2\chi_2(\chi_2-\chi_3)-R_2^2(2+\chi_2)(2+\chi_2+\chi_3)}$

Substitution into (3) and (4) yields the complete solution for the $\boldsymbol{H}$ and $\boldsymbol{B}$ fields. In practice, MRI only measures changes in the local field which are parallel to the large B_0 field. Therefore, the imaged change in local magnetic field in the third region ($r > R_2$) is effectively ΔB_x, given by (7) for an x-directed B_0 field. Defining the main field to be x rather than z directed is unconventional in MRI but, in this analysis, it allows us to retain the usual nomenclature in the cylindrical coordinate system

characterized by $\{r, \phi, z\}$. In the cases of both the gadolinium and SPIO agents, the water region (outside of the NMR vial) was assumed to have a diamagnetic susceptibility of χ_3 =-9.06×10^{-6} and the NMR glass vial, a diamagnetic susceptibility of χ_2 =-9.77×10^{-6}, following the work of Bowen et al. [14]. The theoretical solution of (7) for the gadolinium agent, Magnevist, is plotted in Figure 6(a). For this work, R_1, is 1.715 mm, corresponding to the inner radius of the vials, $R_2 = 2.125$ mm and r represents the cylindrical radial distance measured from the vial's axial center. The main field intensity in A/m is denoted $H_0\,\boldsymbol{i}_x$ and $\varphi = \arctan(y/x)$.

$$\Delta\boldsymbol{B} = \boldsymbol{B} - B_0\boldsymbol{i}_x = \mu_0(1+\chi_3)\frac{D_3}{r^2}\cos\varphi\boldsymbol{i}_r + \mu_0(1+\chi_3)\frac{D_3}{r^2}\sin\varphi\boldsymbol{i}_\varphi \tag{6}$$

$$\begin{aligned}\Delta B_x &= \mu_0(1+\chi_3)\tfrac{D_3}{r^2}\cos^2\varphi - \mu_0(1+\chi_3)\tfrac{D_3}{r^2}\sin^2\varphi \\ &= \mu_0(1+\chi_3)\tfrac{D_3}{r^2}\cos 2\varphi\end{aligned} \tag{7}$$

The expression given by (7), which is the exact solution for ΔB_x when $r > R_2$, differs from the approximate solution supplied by Chu et al. [13] and subsequently used by Bowen et al. [14]. It is the expression of (7) which is used in this work.

It should be apparent that for either a partially or fully magnetically saturated fluid, such as the SPIO Feridex solutions considered in this work, a more general formulation is required where the SPIO magnetization is M_s (as described by the Langevin function but, in practice, a constant at 3 T) in the inner region ($0 < r < R_1$) rather than the linear magnetization susceptibility described by χ_1. In this case, the revised $\boldsymbol{B}$ field for ($0 < r < R_1$) is given by (8) while the $\boldsymbol{H}$ field solution of (3) remains unchanged. The subsequently revised solutions for C_1 through D_3 are as given by Table 1(b). The theoretical solution of (7) for the SPIO agent, Feridex, is plotted in Figure 4(a).

$$\boldsymbol{B}(r,\varphi) = \begin{cases} -\mu_0(C_1 - \frac{D_1}{r^2} - M_s)\cos\varphi\boldsymbol{i}_r + \mu_0(C_1 + \frac{D_1}{r^2} - M_s)\sin\varphi\boldsymbol{i}_\varphi & \text{for} \quad 0 < r < R_1 \\ -\mu_0(1+\chi_2)(C_2 - \frac{D_2}{r^2})\cos\varphi\boldsymbol{i}_r + \mu_0(1+\chi_2)(C_2 + \frac{D_2}{r^2})\sin\varphi\boldsymbol{i}_\varphi & \text{for} \quad R_1 < r < R_2 \\ -\mu_0(1+\chi_3)(C_3 - \frac{D_3}{r^2})\cos\varphi\boldsymbol{i}_r + \mu_0(1+\chi_3)(C_3 + \frac{D_3}{r^2})\sin\varphi\boldsymbol{i}_\varphi & \text{for} \quad r > R_2 \end{cases} \tag{8}$$

The change in ΔB_x for $r > R_2$ is again given by (7) but where D_3 is now revised as indicated in Table 1(b).

The matching of the simulated theoretical field with the experimental results from the MRI was achieved by manually overlapping of the vial's outline in each case for the slice at the vial's axial center. The resultant least-squares fitting was achieved with Matlab (The MathWorks Corp., Natick, MA). Clearly some phase wrapping occurs in the region around the tube as the field varies too rapidly to be captured accurately by the field map. This means that the recorded field immediately surrounding the tube itself is severely distorted from the actual value. However, the dipole fields are closely matched in areas which do not suffer from phase wrapping (e.g., >2cm from the vial's axial center).

3 Results

The results of Figure 4 for the Feridex contrast agent were compared for the line of maximum field variation in the coronal plane (indicated by the black solid line). The results are shown in Figure 5 where the blue solid line indicates the measured result for the change in local Larmor frequency in the water region using MRI, the red line represents a least-squares fit of the MRI result assuming $M_s = 80$ Am^2/kg Fe and the black dashed line represents the result based on the VSM measurement of $M_s = 82$ Am^2/kg Fe. As usual, the Larmor frequency is related to the local magnetic field by the gyromagnetic ratio with a value of 42.58 MHz/T for the ^{1}H proton. Since the simulated dipole distribution shown in Figure 4(a) represents the change in the x component of the B_0 field rather than the magnitude of the magnetic field, the distribution is quadrapolar rather than dipolar as

given by Equation 7 for an infinite cylinder in an x-directed field with finite wall thickness.

Using an identical procedure to that outlined to obtain the results of Figure 4, the B_0 and phase maps were obtained for the Gd-based contrast agent, Magnevist. The theoretical results from Matlab (using the value for the mass susceptibility estimated from the VSM results to be 2.06×10^{-6} m^3/kg Gd) and B_0 map at 3 T are shown in Figure 6. The results in Figure 6 are compared along the line of maximum field variation in the coronal plane, as was the case for the Feridex results. The results are shown in Figure 7 where the blue solid line indicates the measured result for the change in local Larmor frequency using MRI, the red line represents a least-squares fit of the MRI result assuming $\chi_m = 1.96 \times 10^{-6}$ m^3/kg Gd and the black dashed line represents the result from the VSM measurement of $\chi_m = 2.06 \times 10^{-6}$ m^3/kg Gd. It should be noted that the mass susceptibility, χ_m in m^3/kg, is related to the absolute susceptibility, χ (unitless), by the concentration of the magnetic material in the fluid which was 78 kg Gd/m^3.

4 Discussion

Table 2: Comparison of Feridex Results for M_s

VSM Measurement	Fitted MRI Result	Published Result [12]
82 Am^2/kg Fe	80 Am^2/kg Fe	93.6±1.6 Am^2/kg Fe

Table 3: Comparison of Magnevist Results for χ_m

VSM Measurement	Fitted MRI Result	Published Result [11]
2.06×10^{-6} m^3/kg Gd	1.96×10^{-6} m^3/kg Gd	$2.13\pm0.08\times10^{-6}$ m^3/kg Gd

The results for the saturation magnetization of Feridex contrast agent are compared in Table 2 using three different methods. These are (i) the VSM measurements which yielded a result of

82 Am^2/kg Fe at 1.2 T, (ii) the fitted MRI measurement which yielded a value of 80 Am^2/kg Fe at 3 T and (iii) the published result of Jung et al. who cite a result of 93.6 Am^2/kg Fe at 5 T. For the results detailed here, VSM and MRI measurements coincide within 2.5% for Feridex and 5% for Magnevist.

One possible reason for the slight differences between the values of this work and previous result is possible variations in the formulations investigated by earlier workers [11, 12] and this current work which uses commercially available solutions. An explanation for the discrepancy between the MRI and VSM results is possible misalignment between the theoretical and experimental phase maps. This would result in an inaccurate fit of the experimental data (for example, if datapoints closer to the vial tend to suffer more from uncompensated edge effects, this is not reflected in the least-squares fit) and a misalignment between the theoretical result and the MRI measurement (meaning that pixels were not exactly matched in space and therefore introducing an error in the predicted value for the saturation magnetization).

The results for the mass susceptibility of Magnevist contrast agent is compared in Table 3. The comments of the previous paragraph are again applicable. A final note on the Magnevist MRI results is regarding the increased noise in the signal of Figure 7 compared to the Feridex MRI result in Figure 5. This perceived increase in noise is only due to the decreased scale of the local Larmor frequency shown in the Magnevist result rather than due to any increase in the noise inherent to the experiment. The SNR might be improved by increasing the slice thickness and the image FOV albeit leading to the inevitable increase in cylinder end-effects and loss in spatial resolution.

While T1 and T2 are the usual parameters most critical to MR image contrast, there are clinical situations where a measure of the absolute magnetization of the contrast agent is desirable. These include susceptibility-weighted imaging [15, 16] where the local magnetic field is distorted by the magnetization associated with the contrast agent. While the work outlined here details the *in vitro* analysis of the magnetization associated with MRI contrast agents, the work might be extended to *in vivo* studies by examining the flow in long blood vessels where a measurable component of the

B_0 field lies perpendicular to the vessel.

5 Acknowledgments

We gratefully acknowledge the support of the R. J. Shillman Career Development Award, the MIT Buschbaum Fund and the MIT Whitaker Foundation. The project described was supported by Grant Numbers R01 EB007942 and R01 EB006847 from the National Institutes of Health. The authors would like to thank Professor Caroline Ross and Mr. Lei Bi of the Department of Material Sciences and Engineering (MIT) for the use of their VSM in the results of Figure 1 and J. George Hwang in the Department of Electrical Engineering and Computer Science (MIT) for his help with the computational analysis. A final word of thanks is due to the reviewers, in particular for pointing out the diamagnetic properties of the NMR glass tube.

References

[1] Weissleder R, Elizondo G, Wittenberg J, Rabito CA, Bengele HH, Josephson L. Ultrasmall superparamagnetic iron oxide: characterization of a new class of contrast agents for MR imaging. *Radiology.* 1990; **175**: 489-493.

[2] Feridex Patient Information, AMAG Pharmaceutical. *www.berlex.com/html/products/pi/Feridex_PI.pdf*

[3] Bulte JWM, Kraitchman DL. Iron oxide MR contrast agents for molecular and cellular imaging. *NMR Biomed.* 2004; **17**: 484-499.

[4] Kostura L, Kraitchman DL, Mackay AM, Pittenger MF, Bulte JWM. Feridex labeling of mesenchymal stem cells inhibits chondrogenesis but not adipogenesis or osteogenesis *NMR Biomed.* 2004; **17**: 513-517.

[5] Arbab AS, Yocum GT, Rad AM, Khakoo AY, Fellowes V, Read EJ, Frank JA. Labeling of cells with ferumoxides-protamine sulfate complexes does not inhibit function or differentiation capacity of hematopoietic or mesenchymal stem cells. *NMR Biomed.* 2005; **18**: 553-559.

[6] Magnevist Patient Information, Bayer Healthcare.
$http://berlex.bayerhealthcare.com/html/products/pi/Magnevist\_PI.pdf$

[7] Weinmann HJ, Brasch RC, Press WR, Wesbey GE. Characteristics of gadolinium-DTPA complex: a potential NMR contrast agent. *AJR Am J Roentgenol.* 1984; **142**: 619-624.

[8] Wang SC, Wikstrom MG, White DL, Klaveness J, Holtz E, Rongved P, Moseley ME, Brasch RC. Evaluation of Gd-DTPA-labeled dextran as an intravascular MR contrast agent: imaging characteristics in normal rat tissues. *Radiology.* 1990; **175**: 483-488.

[9] Gillis P, Koenig SH. Transverse Relaxation of Solvent Protons Induced by Magnetized Spheres: Application to Ferritin, Erthrocytes and Magnetite, *Magn Reson Med*, 1987; **5**: 232-245.

[10] Zahn M. *Electromagnetic Field Theory: a problem solving approach.* Florida: Krieger Publishing Company, 2003.

[11] Weisskoff R, Kiihne S. MRI Susceptometry: Image-Based Measurement of Absolute Susceptibility of MR Contrast Agents and Human Blood. *Magn Reson Med,* 1992; **24**: 375-383.

[12] Jung CW, Jacobs P. Physical and Chemical Properties of Superparamagnetic Iron Oxide MR Contrast Agents: Ferumoxides, Ferumoxtran, Ferumoxsil. *Magn Reson Imaging*, 1994; **13**: 661-674.

[13] Chu SC-K, Xu Y, Balschi JA, Springer CS. Bulk Magnetic Susceptibility Shifts in NMR Studies of Compartmentalized Samples: Use of Paramagnetic Reagents. *Magn Reson Med*, 1990, **13**: 239-262.

[14] Bowen CV, Zhang X, Saab G, Gareau PJ, Rutt BK. Application of the Static Dephasing Regime Theory to Superparamagnetic Iron-Oxide Loaded Cells. *Magn Reson Med*, 2002, **48**: 52-61.

[15] Haacke EM, Lai S, Reichenbach JR, Kuppusamy K, Hoogenraad FGC, Takeichi H and Lin W. *In vivo* measurement of blood oxygen saturation using magnetic resonance imaging: a direct validation of the blood oxygen level-dependent concept in functional brain imaging. *Hum Brain Mapp,* 1997; **5**: 341-346.

[16] Tong KA, Ashwal S, Obenaus A, Nickerson JP, Kido D, Haacke EM. Susceptibility-Weighted MR Imaging: A Review of Clinical Applications in Children. *Am J Neuroradiol,* 2007; **29**: 9.

[17] Schenck JF. The role of magnetic susceptibility in magnetic resonance imaging: MRI magnetic compatibility of the first and second kinds. *Med Phys.* 1996; **23**: 815-850.

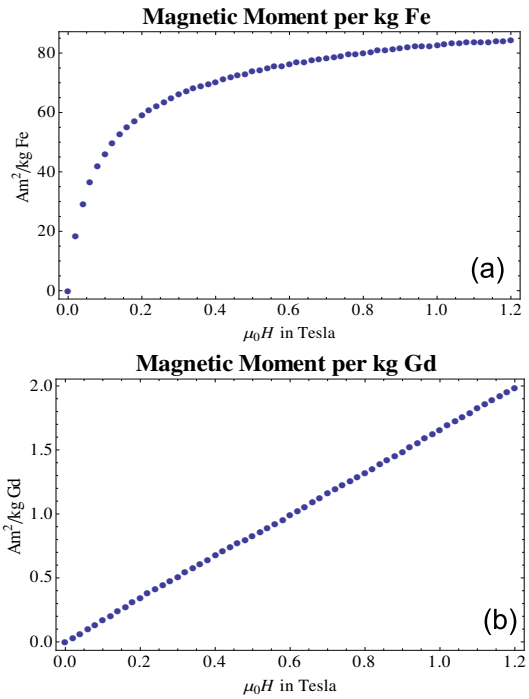

Figure 1: Measured magnetization using a VSM for (a) Feridex and (b) Magnevist MRI contrast agents. The units of magnetic moment are (a) $\mathrm{Am}^2/\mathrm{kg}$ Fe for Feridex and (b) $\mathrm{Am}^2/\mathrm{kg}$ Gd for Magnevist.

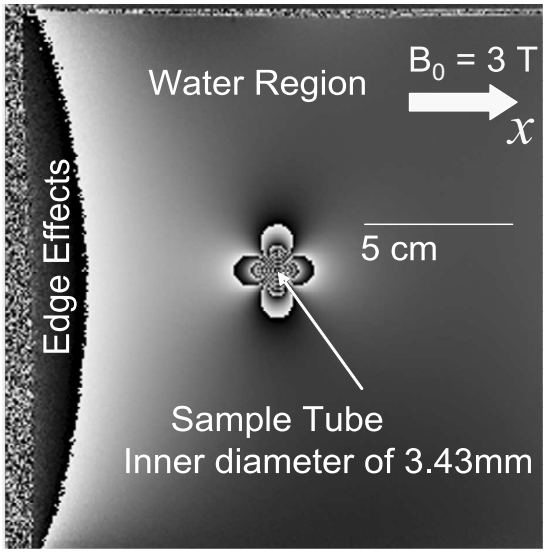

Figure 2: The measured phase map is shown for the center coronal slice of a tube of Feridex agent surrounded by water. The phase map only shows the net field component along the x-axis, *i.e.*, B_x. The B_0 field is left to right (x-directed) and has a value of 3 T.

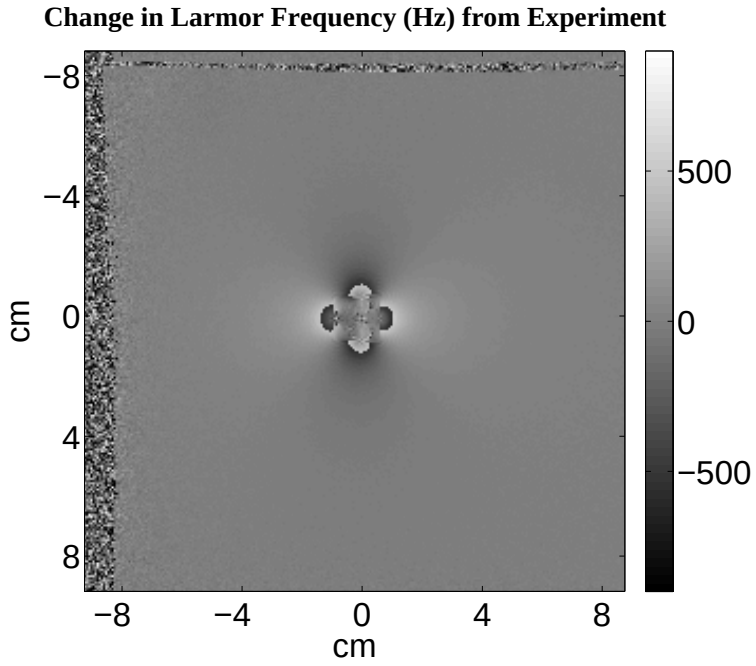

Figure 3: The B_0 map is shown for the center coronal slice of a tube of Feridex agent surrounded by water. Edge and shim effects were eliminated by means of a subtraction of the B_0 maps measured in the absence of any tube.

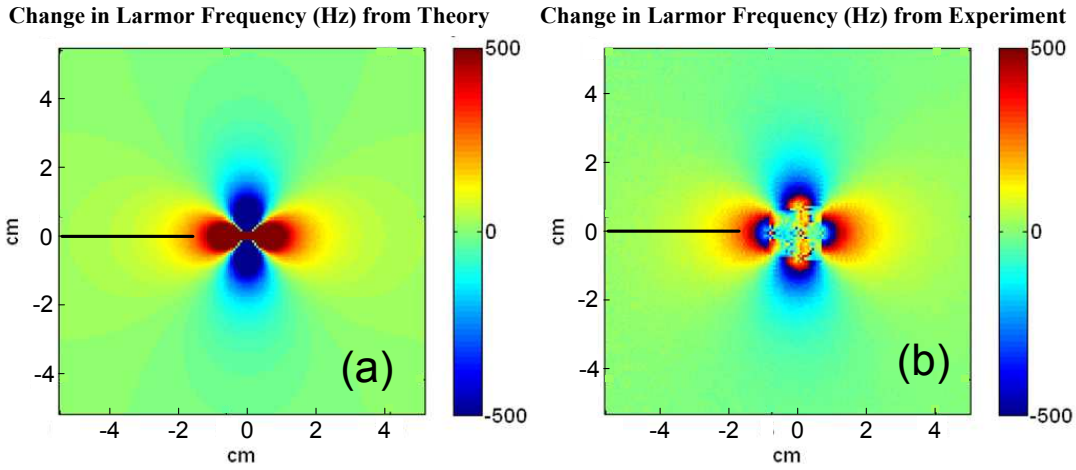

Figure 4: Comparing Feridex contrast agent (a) theoretical results from Eq. (7) and (b) B_0 maps from the scanner at 3 T. The black line indicates the line of maximum field variation.

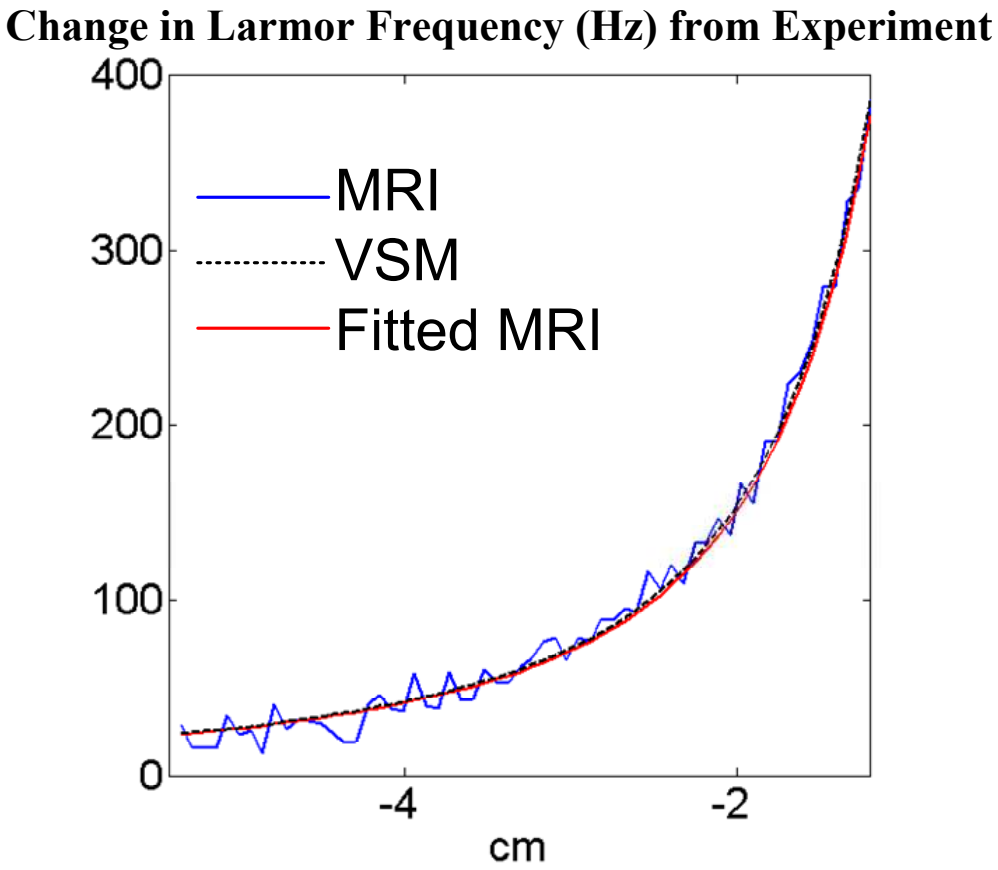

Figure 5: Comparing experimental results for Feridex contrast agent from the MRI (blue), results from the VSM at 1.2 T (black dashed) and theoretical results from Comsol Multiphysics (red) based on a least-squares fit of the MRI data for the change in local Larmor frequency due to the SPIO agent, Feridex at 3T. The x axis corresponds to the solid black lines in Figure 4.

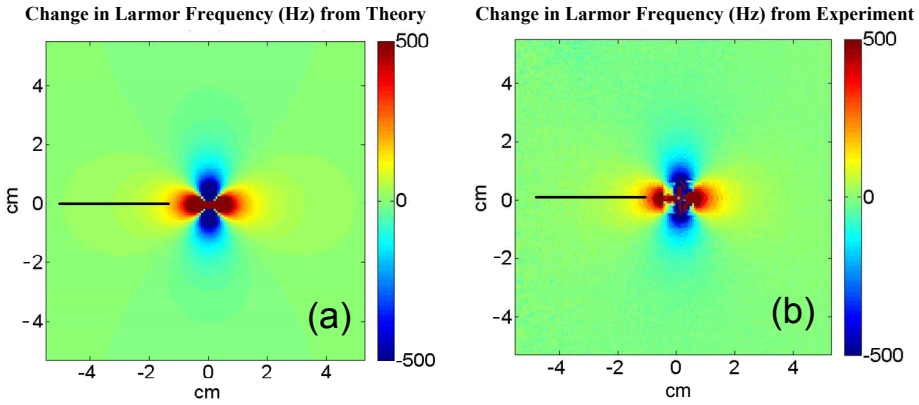

Figure 6: Comparing for Magnevist contrast agent (a) theoetical results from Eq. (7) and (b) B_0 maps from the MRI at 3 T for Magnevist contrast agent.

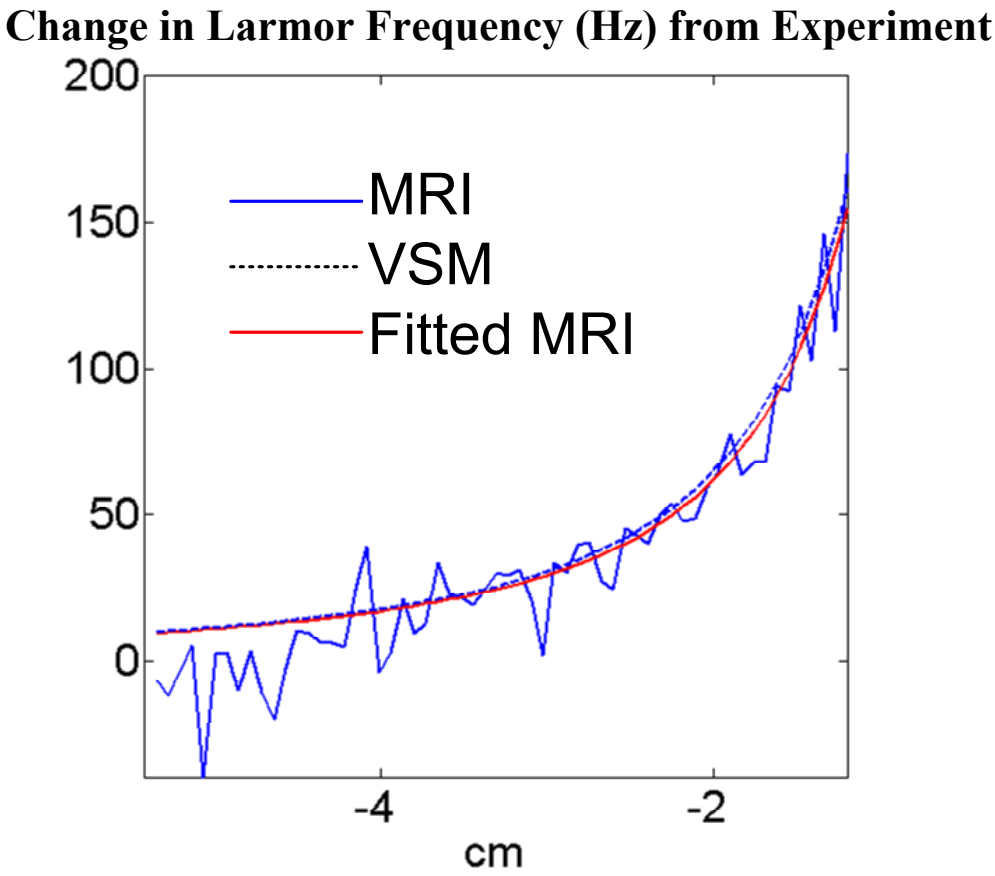

Figure 7: Comparing experimental results for Magnevist from the MRI (blue), extraopolated results from the VSM at 1.2 T (black dashed) and theoretical results from Eq. (7) (red) based on a least-squares fit of the MRI data for the change in local Larmor frequency at 3T. The x axis corresponds to the solid black lines in Figure 6.